MRS Advances (2025) 10:1767–1772
https://doi.org/10.1557/s43580-025-01382-w

ORIGINAL PAPER

A dilatometer and *in situ* synchrotron X-ray diffraction study: α-quenching and reheating of a Nb-rich titanium aluminide alloy

Andreas Stark[1] · Dieter Lott[1] · Florian Pyczak[1]

Received: 14 January 2025 / Accepted: 18 August 2025 / Published online: 2 September 2025

Abstract
Intermetallic γ-TiAl-based alloys are currently used as structural materials for turbine blades in aero engines. Additive manufacturing is increasingly considered as an additional manufacturing route for components consisting of γ titanium aluminides; however, the high heating and cooling rates result in chemical and thermodynamical disequilibrated microstructures. In our study, *in situ* synchrotron X-ray diffraction was applied to follow the formation of the disequilibrium microstructure during quenching and to study its re-equilibration during a subsequent annealing treatment in a Nb-rich γ-TiAl-based alloy. The quenched sample showed an incomplete massive transformation, with large remaining α_2 grains. During reheating, the analysis of the collected data showed that equilibration of the quenched microstructure takes place in several reordering and transformation steps, e.g., orthorhombic distortion of the hexagonal α_2 phase (around 550 °C), almost complete transformation of the supersaturated quenched α_2 to γ (around 850 °C), and retransformation of γ to new α_2 (around 1050 °C).

Introduction

Intermetallic γ-TiAl-based alloys have been successfully introduced as structural materials for low-pressure turbine blades in civil aero engines during the last decade [1]. A possibility to expand the range of their use is the introduction of novel production methods like additive manufacturing (AM). A challenge of AM processes is the very fast cooling and heating rates that cause the formation of microstructures far away from chemical and thermodynamic equilibrium. To equilibrate the microstructure, a subsequent heat treatment is necessary.

Intermetallic γ-TiAl-based alloys are multiphase alloys [2]. In the binary system Ti–Al, they consist of tetragonal γ TiAl phase (P4/mmm; $L1_0$) and hexagonal α_2 Ti_3Al phase ($P6_3/mmc$; $D0_{19}$). At high temperatures, ordered α_2 disorders to hexagonal α Ti(Al) phase ($P6_3/mmc$; A3). Advanced titanium aluminides contain additional alloying elements like Nb. The addition of Nb improves the mechanical properties and the oxidation resistance. On the other hand, Nb stabilizes additional phases like ω_o phase [3] and O phase [4] and the decelerated diffusion due to Nb facilitates massive transformation even at moderate cooling rates [5].

The phase transformation pathways involved in the AM process of γ-TiAl-based alloys are difficult to understand using conventional characterization and analysis methods solely based on the resulting microstructures. In contrast, *in situ* high-energy X-ray diffraction experiments using synchrotron radiation enable a highly time-resolved and direct observation of the evolution of phases during this dynamic process. The aim of this study is to investigate the formation of disequilibrium conditions and the subsequent equilibration process during annealing in a high Nb-containing γ-TiAl-based alloy.

Experimental

The present study uses a relatively well-investigated Nb-rich ternary model alloy with a nominal composition of Ti-46Al-9Nb (in at.%) [6, 7]. The alloy was powder metallurgically produced, which ensures a high chemical homogeneity. The hot isostatically pressed sample had a fine-grained "near gamma" microstructure with globular γ grains (5–10 µm) and a small amount of α_2 phase at triple points [6].

The heat treatments were performed with a quenching dilatometer DIL805A/D that can run in the HEMS beamline

✉ Andreas Stark
andreas.stark@hereon.de

[1] Institute of Materials Physics, Helmholtz-Zentrum Hereon, Geesthacht, Germany

P07B operated by Hereon in the PETRA III synchrotron ring at DESY. Debye Scherrer diffraction rings were recorded continuously on a Varex XRD 4343RF flat panel detector with a pixel size of 150 µm × 150 µm and 2880×2880 pixels during the heat treatments. Exposure times of 0.1 s, 1 s , and 2 s were used for the various required time resolutions. The beam had a photon energy of 87.1 keV, corresponding to a wavelength of 0.14235 Å, and a spot size of 0.5 mm × 0.5 mm. Sample-detector distance and beam center were calibrated using a LaB_6 powder standard.

In order to reach a high quenching rate, a hollow cylindrical sample was used with 10 mm length, an outer diameter of 5 mm, and a 2 mm hole. Thus, it can be cooled from outside as well as from inside (!) by blowing with He gas. The sample was heated inductively controlled by a spot-welded Type S thermocouple. Two heat treatments were performed. In the first "α-quenching" treatment, the sample was heated with a rate of 2 °C/s to 1350 °C in the α single-phase field and, after a short dwell time of 30 s, quenched as fast as possible in order to freeze the high-temperature condition. Therefore, the high-frequency generator was switched off and the He gas valve was opened to its maximum, which leads to a quenching rate of about 500 °C/s within the first 1.5 s down to temperatures below 600 °C. In the second "reheating" treatment, the sample was slowly heated at a rate of 10 °C/min to 1250 °C and, after a dwell time of 5 min, cooled to room temperature at the same rate.

The measured diffraction rings were azimuthally integrated using pydidas [8] and the resulting diffraction patterns were analyzed by Rietveld refinement using MAUD [9]. As the grain statistics deteriorated during the first heat treatment due to grain coarsening, selected diffraction peaks were also fitted using a Gaussian in addition to Rietveld refinement. In this way, qualitative statements regarding the reordering and transformation steps during reheating could be made.

Results and discussion

Phase transformations during the α-quenching heat treatment

Figure 1 shows diffraction images taken during the α-quenching heat treatment. At the beginning (Fig. 1a) continuous diffraction rings indicate a fine-grained microstructure. Rietveld analysis results in a phase constitution of about 95 vol.% γ and 5 vol.% α_2. During heating, the α_2 101 reflection vanishes at 1201 °C, indicating the order–disorder transformation $\alpha_2 \leftrightarrow \alpha$. At 1335 °C , the γ phase dissolves. In the α single-phase field, a significant grain coarsening sets in. Thus, at the end of the 30-s segment at 1350 °C, only a few strong α reflection spots remain visible in the diffraction image (Fig. 1b). Then the sample was quenched as fast as possible at a rate of about 500 °C/s within the first

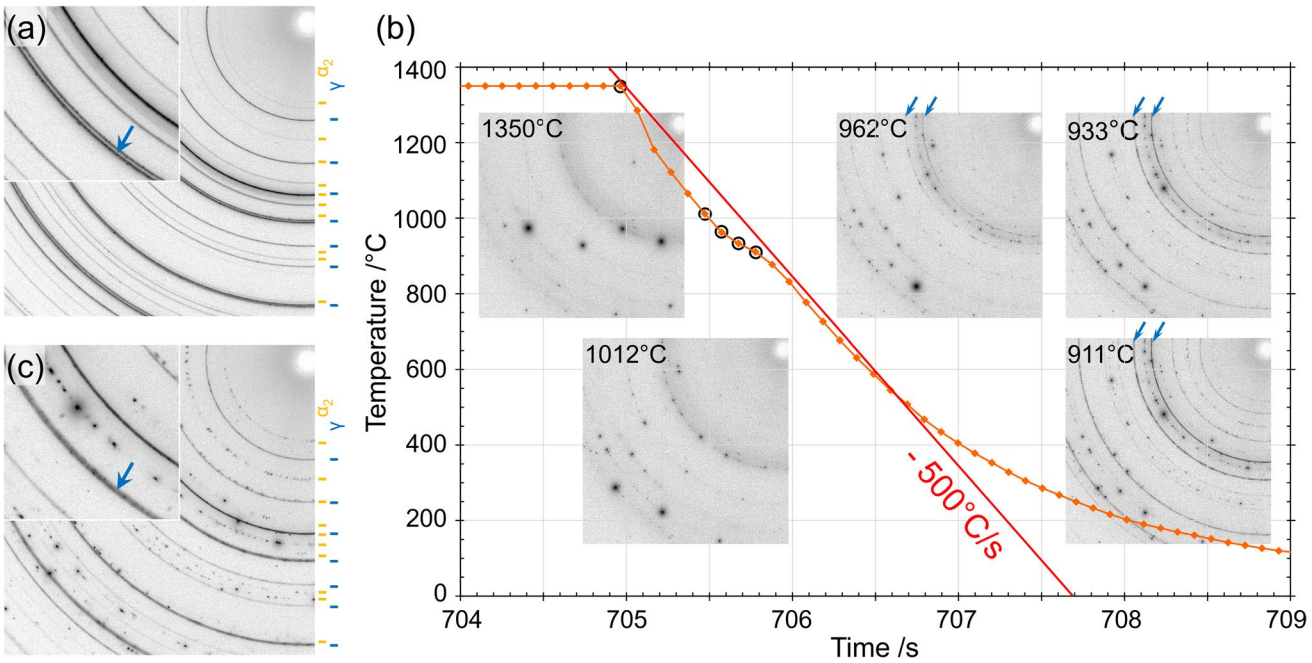

Fig. 1 Quarters of the diffraction rings of the α-quenching heat treatment. **a** At room temperature before heat treatment started. **b** During the first seconds of the quenching. **c** At room temperature after heat treatment ended. (Blue arrows point to exemplary γ rings. In **a** and **c** the rings are assigned to the corresponding phases.)

1.5 s (Fig. 1b). During this quenching, a part of the α phase massively transforms to γ_m phase. This transformation takes place within a few tenths of a second in the temperature range just below 1000 °C. First, weak γ reflections appear at 962 °C, while 0.2 s, later at 911 °C 50% and 1 s later at 545 °C, more than 80% of the massive transformation is already completed. The transformation $\alpha \rightarrow \gamma$ is an exothermic reaction as the temporary decrease of the quenching rate shows that appears during the main part of the transformation happens (Fig. 1b). The massive transformed γ_m again forms continuous diffraction rings, indicating a fine-grained microstructure without preferred crystallographic orientations demonstrating that no crystallographic orientation relationship of γ_m to the coarse α grains exists. At the same time as the massive transformation, the ordering $\alpha \rightarrow \alpha_2$ takes place, which in turn results in an increase of the number of spots on the α/α_2 rings due to the formation of anti-phase domains. At the end of the heat treatment (Fig. 1c), the sample again consists of γ and α_2. However, compared to the starting microstructure now (i) the amount of γ is smaller with about 45 vol.%, (ii) the α_2 grains are larger, as evidenced by the very spotty α_2 diffraction rings, and (iii) the *c/a* ratio of the tetragonal γ phase is significantly smaller, indicated by the disappearance of the peak splitting of, e.g., the γ 002 and γ 200 reflections (blue arrows in Fig. 1a, c). The small *c/a* ratio is a typical feature of γ_m and can be attributed to the high disorder in the γ TiAl crystal lattice caused by the high transformation speed of the massive transformation [7].

While it is reported that oil quenching of 1 mm thick sheet specimens, which were annealed in a furnace for 7 min at 1330 °C, results in a fully massive transformation [5], in this study only around 45 vol.% of the α phase transforms to γ_m. One reason can be, that the applied quenching rate of 500 °C/s is higher than that of oil quenching, which can be estimated at around 100 °C/s. Thus, a high amount of high-temperature α is frozen before it can transform to γ_m. Additionally, the relatively coarse α grain structure can play a role. In the cited study of Bartels et al. [5] grain coarsening was restricted to about 100 µm due to the chosen maximum heat treatment temperature just below the γ solvus temperature. Because massive transformation starts at the grain boundaries, the smaller α grains can completely transform into γ_m.

Phase transformations during the reheating process

Figure 2 shows the evolution of peak intensities and peak widths of characteristic diffraction peaks of α_2 and γ phase, as well as of the *c/a* ratio of γ and the interatomic distance in the basal plane of α/α_2 phase during reheating. Depending on the evolution of these parameters, the reheating process can be divided into 6 stages. Figure 3 shows the characteristic diffraction images of these different stages.

In the first stage up to about 460 °C, the microstructure does not change. The phase contents remain at 45 vol.% γ_m and 55 vol.% α_2. Since the Rietveld refinement does not deliver reliable values due to the insufficient grain statistics of α_2, the phase content is estimated based on the integral intensity of various γ peaks.

In stage 2 between 460 °C and 660 °C, a significant peak broadening of α_2 reflections occurs (Fig. 2b). In the corresponding diffraction image (Fig. 3b), the α_2 reflections appear rod-shaped. This is the typical appearance of an orthorhombic distortion in the hexagonal basal plane of α_2 [4] which results in a splitting of α_2 reflections that contain the a lattice parameter (e.g., 200, 201, …). The splitting of one α_2 peak into two peaks with slightly different 2 θ angles results in a rodlike shape in the diffraction image or in an increasing peak width and a simultaneous decrease of the peak maximum in the fitted Gauss curve. Above 660 °C the distortion disappears again. The reason for this orthorhombic distortion may be the formation of orthorhombic O phase which is a stable phase at low temperatures in high Nb-containing γ TiAl-based alloys [10]. The high degree of disorder in the quenched α_2 phase might facilitate the formation of orthorhombic O phase compared to the ordering of α_2 phase.

Between 660 °C and 750 °C in stage 3 the microstructure resembles the one in stage 1 as the quasi-identical diffraction images taken at 22 °C (Fig. 3a) and 710 °C (Fig. 3c) demonstrate.

Starting from 750 °C, the peak width significantly increases in α_2 as well as in γ (Fig. 2b). Simultaneously, the peak intensity of α_2 starts to decrease and reaches a minimum around 950 °C, indicating an almost complete transformation of the quenched α_2 to γ in stage 4. In the diffraction image (Fig. 3d), pronounced streaks are visible not only in α_2 but also in γ. While the peak width of γ reaches a maximum quite quickly (around 800 °C), the peak width of α_2 continues to rise until almost 950 °C. All these features indicate that γ lamellae start to grow in the quenched α_2 grains. The temperature range around 800 °C is the typical range for the formation of γ lamellae in supersaturated quenched α_2 grains [11]. Fine lamellar crystallites result in streaky reflections in the reciprocal space and thus in an increased peak width. Being quite thin at the beginning, the emerging lamellae of γ in the α_2 grains grow rapidly. This results in an early peak maximum and a subsequent decrease of the γ peak width (Fig. 2b). On the other hand, the remaining α_2 lamellae between the γ lamellae are getting thinner and thinner, which leads to a continuous increase of the α_2 peak width until the end of stage 4.

At the beginning of stage 4, the *c/a* ratio of γ increases slightly, but it still remains at a rather low level (around

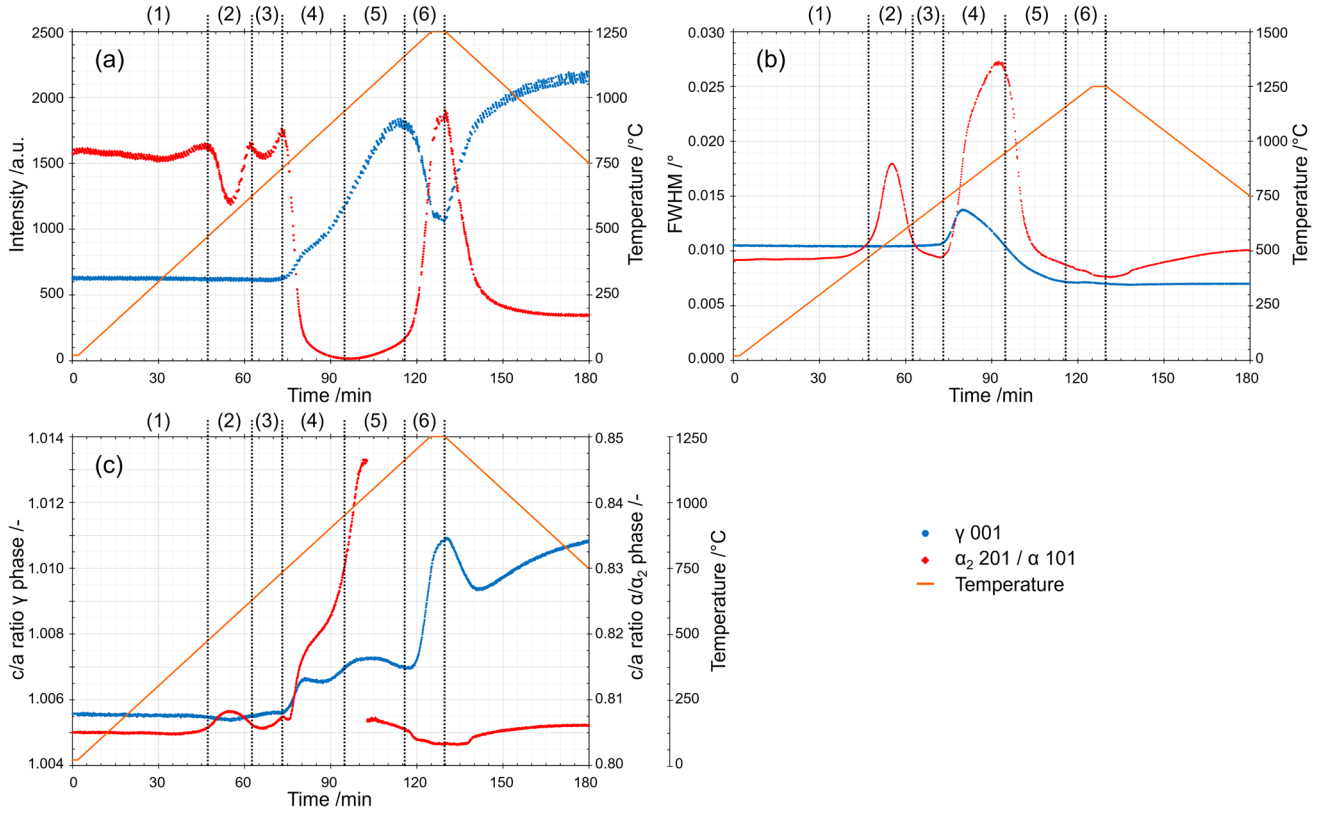

Fig. 2 Evolution of **a** peak intensity and **b** peak width of characteristic diffraction peaks of α_2 and γ phase, and of **c** *c/a* ratio of γ and interatomic distance in the basal plane of α/α_2 phase during reheating. The reheating process can be divided in 6 stages depending on the evolution of these parameters

1.007) in the further course of stages 4 and 5. In Fig. 3e, already two rings are distinguishable for γ 002 and γ 200 (blue arrow in Fig. 3e) compared to the blurred broad single ring in the massive transformed condition. This means the degree of disorder in γ_m decreases but γ has not yet assumed its final tetragonal condition. A similar behavior was observed by Bartels et al. [5] and Liss et al. [7]; however, they reheated samples which before underwent a complete massive transformation (100 vol.% γ_m).

Stage 5 is generally characterized by the decrease of the peak widths in both phases and a slight increase of the α_2 peak intensity, which means a slightly increasing α_2 phase fraction. The most striking feature, however, is the steep increase of the interatomic distance in the basal plane of α_2 (Fig. 2c) corresponding to a change in the *a* lattice parameter of α_2. In fact, two types of α_2 phases with different *a* lattice parameters seem to coexist for some time. Thus, the lattice parameter does not change abruptly, but the abrupt change visible in Fig. 2c is an artifact due to the fitting with a single Gaussian. Figure 3e shows a weak continuous α_2 201 ring beside two pale α_2 201 spots at slightly larger radial distance which corresponds to the 2 θ angle (red arrows in Fig. 3e). The pale α_2 spots stem from remaining supersaturated quenched α_2 grains while the weak continuous α_2 ring is formed by the newly grown α_2 crystals. This indicates that new α_2 crystallites grow at γ grain boundaries without an orientation relationship to γ. The reason for the different *a* lattice parameters is caused by a compression of the basal plane of the quenched α_2 grains during the growth of the γ lamellae in stage 4. During this growth, the close-packed planes of both phases, {111}γ and {0001}α_2, are oriented parallel to each other and seem to be fully or partly coherent. However, the average interatomic distance in {111}γ is slightly smaller than in {0001}α_2. The thinner the remaining α_2 lamellae become, the more the atoms in their basal planes are forced to approach the interatomic distances in the {111}γ planes. This results in a decrease of the α_2 *a* lattice parameter since the newly growing α_2 crystallites without an orientation relationship to γ are no longer compressed by the surrounding γ lattice.

With the beginning of stage 6 above 1160 °C, the volume fraction of α_2 starts to increase while that of γ decreases significantly. At the same time, the *c/a* ratio of γ starts to increase which is very pronounced especially after the disorder transformation $\alpha_2 \rightarrow \alpha$ finished at around 1200 °C (Fig. 2c). This indicates that diffusion, now at the high

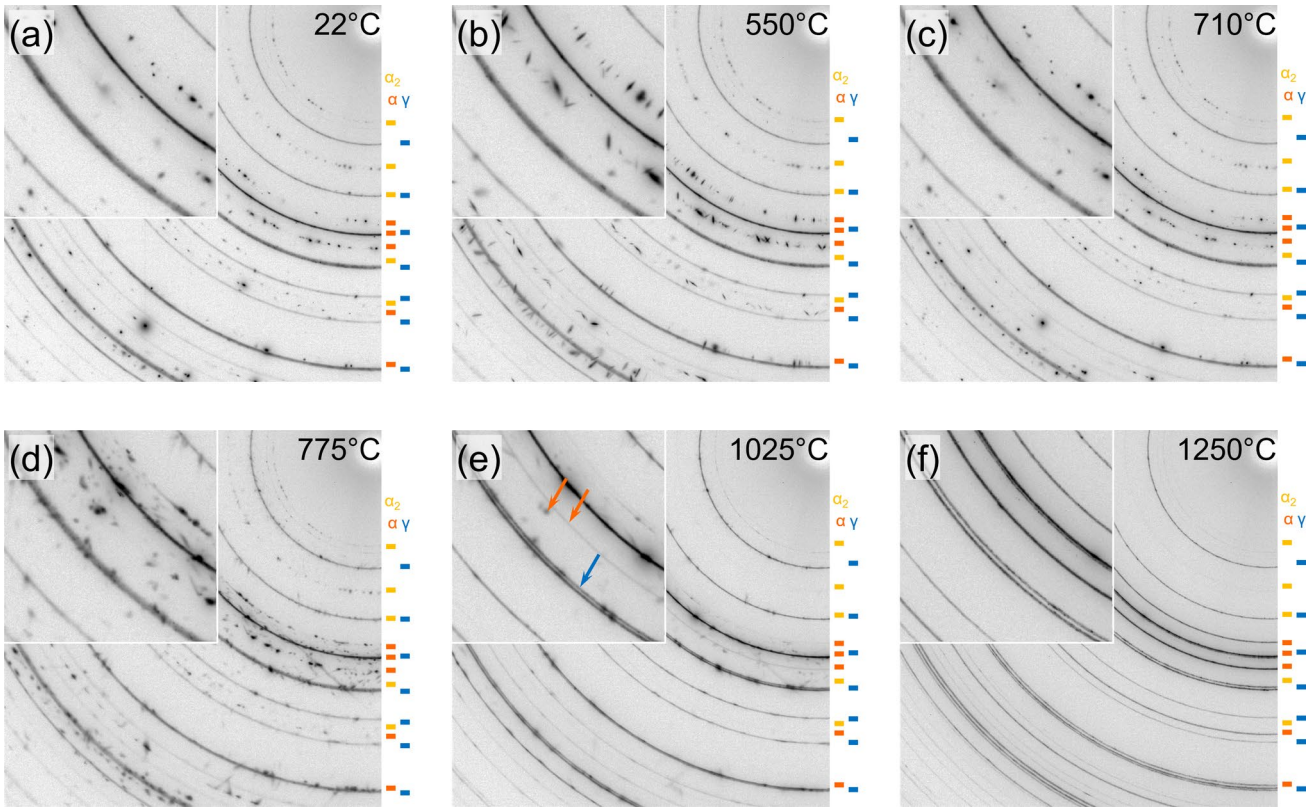

Fig. 3 Characteristic diffraction images of the different stages during reheating. In (**e**) the blue arrow marks the γ 002 and γ 200 double ring and the red arrows mark pale α_2 spots and a pale α_2 ring

temperatures, plays a prominent role because gamma can only reach its equilibrium *c/a* ratio by assuming its chemical equilibrium composition and increasing its degree of order and thus its tetragonality. The fact that the intermetallic (partly covalent) bonding in α_2 is no longer present may additionally facilitate diffusion. At the end of the 5 min dwell time at 1250 °C, the sample is almost back in thermodynamic and chemical equilibrium. The continuous rings (Fig. 3f) indicate again a relatively fine-grained microstructure, and the phase fractions can be determined to 58 vol.% γ and 42 vol.% α.

Conclusions

In situ synchrotron X-ray diffraction experiments during α-quenching and reheating of a Nb-rich titanium aluminide alloy show:

- 500 °C/s quenching rate is not fast enough to freeze the high-temperature condition completely in Nb-rich TiAl alloys.
- Equilibration of the quenched condition takes place in several reordering and transformation steps during reheating.

These results provide new insights into the formation of disequilibrium conditions during AM-like quenching and their equilibration during subsequent annealing treatments in Nb-rich γ-TiAl-based alloys.

Acknowledgments The support of Emad Maawad and Tim Lengler during the experiments is gratefully acknowledged.

Author contributions A.S. performed the experiments, analyzed the data, and drafted the manuscript. All authors discussed the results and commented on the manuscript.

Funding Open Access funding enabled and organized by Projekt DEAL. No funding was received for conducting this study.

Data availability Data will be made available upon reasonable request.

Declarations

Conflict of interest On behalf of all authors, the corresponding author states that there is no conflict of interest.

References

1. B.P. Bewlay, S. Nag, A. Suzuki, M.J. Weimer, Mater. High Temp. **33**, 549–559 (2016). https://doi.org/10.1080/09603409.2016.1183068
2. F. Appel, J.D.H. Paul, M. Oehring, *Gamma titanium aluminide alloys* (Wiley, Weinheim, 2011). https://doi.org/10.1002/9783527636204
3. A. Stark, A. Bartels, H. Clemens, F.-P. Schimansky, Adv. Eng. Mater. **10**, 929–934 (2008). https://doi.org/10.1002/adem.200800188
4. M.W. Rackel, A. Stark, H. Gabrisch, N. Schell, A. Schreyer, F. Pyczak, Acta Mater. **121**, 343–351 (2016). https://doi.org/10.1016/j.actamat.2016.09.030
5. A. Bartels, S. Bystrzanowski, H. Chladil, H. Leitner, H. Clemens, R. Gerling, F.-P. Schimansky, Mater. Res. Soc. Symp. Proc. **842**, 193–198 (2005)
6. R. Gerling, A. Bartels, H. Clemens, H. Kestler, F.-P. Schimansky, Intermetallics **12**, 275–280 (2004). https://doi.org/10.1016/j.intermet.2003.10.005
7. K.-D. Liss, A. Bartels, H. Clemens, S. Bystrzanowski, A. Stark, T. Buslaps, F.-P. Schimansky, R. Gerling, C. Scheu, A. Schreyer, Acta Mater. **54**, 3721–3735 (2006). https://doi.org/10.1016/j.actamat.2006.04.004
8. M. Storm, Python Diffr. Data Anal. Suite (2024). https://doi.org/10.5281/zenodo.7568610
9. L. Lutterotti, R. Vasin, H.-R. Wenk, Powder Diffr. **29**, 76–84 (2014). https://doi.org/10.1017/S0885715613001346
10. M.W. Rackel, A. Stark, H. Gabrisch, F. Pyczak, Intermetallics **131**, 107086 (2021). https://doi.org/10.1016/j.intermet.2021.107086
11. L. Cha, T. Schmoelzer, Z. Zhang, S. Mayer, H. Clemens, P. Staron, G. Dehm, Adv. Eng. Mater. **14**, 299–303 (2012). https://doi.org/10.1002/adem.201100272